

# Efficient Bearing Sensor Data Compression via an Asymmetrical Autoencoder with a Lifting Wavelet Transform Layer

Xin Zhu

Department of Electrical and Computer Engineering  
University of Illinois Chicago  
Chicago, IL, USA  
xzhu61@uic.edu

Ahmet Enis Çetin

Department of Electrical and Computer Engineering  
University of Illinois Chicago  
Chicago, IL, USA  
aecy@uic.edu

**Abstract**—Bearing data compression is vital to manage the large volumes of data generated during condition monitoring. In this paper, a novel asymmetrical autoencoder with a lifting wavelet transform (LWT) layer is developed to compress bearing sensor data. The encoder part of the network consists of a convolutional layer followed by a wavelet filterbank layer. Specifically, a dual-channel convolutional block with diverse convolutional kernel sizes and varying processing depths is integrated into the wavelet filterbank layer to enable comprehensive feature extraction from the wavelet domain. Additionally, the adaptive hard-thresholding nonlinearity is applied to remove redundant components while denoising the primary wavelet coefficients. On the decoder side, inverse LWT, along with multiple linear layers and activation functions, is employed to reconstruct the original signals. Furthermore, to enhance compression efficiency, a sparsity constraint is introduced during training to impose sparsity on the latent representations. The experimental results demonstrate that the proposed approach achieves superior data compression performance compared to state-of-the-art methods.

**Index Terms**—Asymmetrical autoencoder, bearing sensor data compression, lifting wavelet transform, adaptive hard-thresholding nonlinearity.

## I. INTRODUCTION

Bearings play a critical role in various mechanical systems, facilitating both rotational and linear motion with diminished friction [1]. Monitoring and analyzing the condition of bearings is crucial for maintaining the reliability and operational efficiency of mechanical systems, as undetected bearing failures can result in substantial downtime, costly repairs, and potentially catastrophic system failures [2]. However, condition monitoring techniques, such as vibration analysis and acoustic emission methods [3], [4], generate large volumes of data over time, which presents challenges for rapid transmission and real-time analysis in bandwidth-constrained environments.

Bearing data compression mitigates these challenges by minimizing the data volume while retaining essential information required for precise analysis and fault diagnosis.

This work was supported by the National Science Foundation (NSF) under grant 2303700. AE Cetin is also funded by the DoE Award Number: DE-SC0023715.

Vibration data compression methods can generally be divided into lossless and lossy compression techniques.

Lossless compression methods reduce data size without any loss of information [5]–[7]. Huang *et al.* proposed a divide-and-compress lossless compression scheme [8]. The discrete cosine transform (DCT) is used to partition the bearing data into two segments: the first consists of a few DCT coefficients that capture the majority of the signal’s energy, while the second part contains high-frequency DCT coefficients that represent widely dispersed differences with minimal energy. Next, distinct encoding strategies are implemented for each short-time segment according to their unique data properties. However, it has a low compression efficiency.

Lossy data compression techniques achieve higher compression ratios by eliminating redundancy, potentially resulting in a reduction in quality [9]–[11]. In many practical applications, there is no need to compress the data in a lossless manner [12], [13]. In [14], a three-dimensional vibration data compression method was developed by incorporating the dimensions of length, width, and height to enhance compression efficiency. Guo *et al.* proposed an optimal ensemble empirical mode decomposition (EEMD) based bearing data compression approach. It extracts the intrinsic mode function associated with bearing faults and compresses this component, rather than the original signal, to improve compression ratio [15]. Additionally, an asymmetrical autoencoder was designed to compress vibration signals [16]. It introduces a sparsifying discrete cosine Stockwell transform layer to eliminate redundant data and capture important features in the latent space. The DCT-based lossy compression methods have a low reconstruction accuracy compared to the proposed wavelet transform-based method (this article).

To address the challenges of low reconstruction accuracy in lossy compression methods and the inefficiency of lossless compression techniques, this paper presents an asymmetrical autoencoder with a lifting wavelet transform layer (AAELWTL) for compressing bearing sensor data. The encoder module is designed with low complexity to facilitate implementation on sensors, while the decoder module incor-

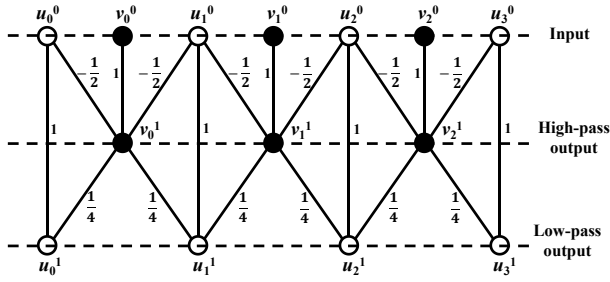


Fig. 1. Lifting low-pass and high-pass filtering steps for the (5, 3) Daubechies biorthogonal filterbank.

porates a more complex structure to improve reconstruction accuracy. Specifically, a novel lifting wavelet transform (LWT) layer is introduced in the encoder to extract an efficient latent space representation. The key idea of the LWT layer is to leverage convolutional layers to capture important frequency domain features while an adaptive hard-thresholding layer is applied to eliminate redundant data and appropriately scale (denoise) the large coefficients. In the decoder, the inverse LWT (ILWT) is combined with three linear layers to reconstruct the original signals. Additionally, a sparsity penalty is integrated into the training process to enforce sparsity on the latent space coefficients, further optimizing the compression efficiency. The proposed model exhibits superior compression efficiency and reconstruction accuracy compared to other state-of-the-art models, as demonstrated on two bearing datasets: the MFPT [17] and XJTU [18] datasets.

## II. PRELIMINARIES

LWT is used in a wide range of applications, including the JPEG 2000 image compression standard [19]–[25]. In LWT, the low-pass and high-pass filtering operations are applied to the input after the lazy filterbank, which decomposes the input samples into even-indexed components, denoted as  $u_i^0$ , and odd-indexed components, denoted as  $v_i^0$ . For the (5, 3) filter bank [20], the highpass-filtered sub-signal  $v_i^1$  is obtained by estimating each odd-indexed sample as a linear combination of two neighboring even-indexed samples and calculating the difference as follows:

$$v_i^1 = v_i^0 - 0.5(u_i^0 + u_{i+1}^0) \quad (1)$$

where  $i$  is the sample index. The low-pass filtered sub-signal  $u_i^1$  is obtained using the update step:

$$u_i^1 = u_i^0 + 0.25(v_i^1 + v_{i-1}^1) \quad (2)$$

This process is illustrated in Fig. 1.

## III. ASYMMETRICAL AUTOENCODER WITH A LIFTING WAVELET TRANSFORM LAYER

The asymmetrical autoencoder is a variant of the traditional autoencoder architecture, where the encoder and decoder have different levels of complexity. In the realm of data compression, this asymmetry typically involves a more complex encoder designed to extract features and compress

signals efficiently [26]. However, the complex encoder requires substantial computational resources. It poses a challenge for deploying autoencoders in low-cost sensor applications, where minimizing resource consumption is critical.

### A. Structure of AAELWTL

Unlike the established asymmetrical autoencoder [26], the AAELWTL encoder is developed with low computational complexity for implementation in the sensor, while the decoder incorporates more sophisticated architectures to enhance data reconstruction accuracy. This approach is viable as the decoder operates on a high-performance host computer, capable of handling higher computational workloads than the sensor.

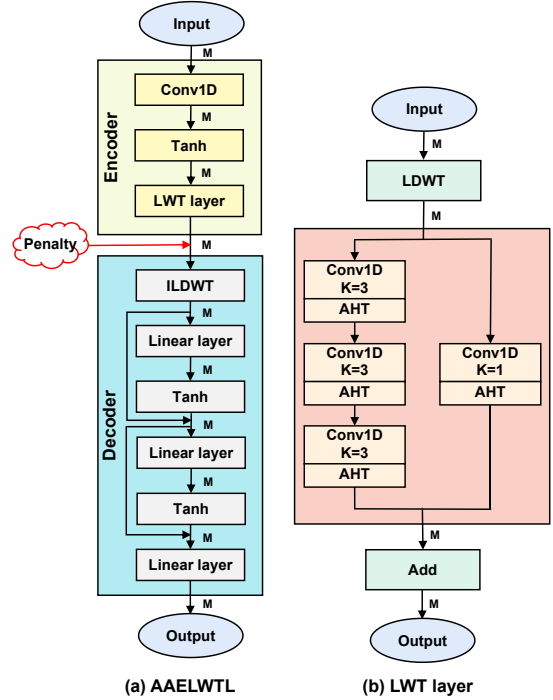


Fig. 2. Block diagrams of the AAELWTL and LWT layer.

### Encoder Module of the AAELWTL:

The bearing signal is divided into short-time segments, each with a duration of  $M$  samples. Here, we choose  $M = 7$  because a small segment length minimizes computational cost and reduces the number of trainable parameters. As is shown in Fig. 2, each data segment is passed through a convolutional layer, followed by a tanh activation function. The output from the tanh function is denoted as  $\mathbf{x} \in \mathbb{R}^M$ . Next, the LWT of  $\mathbf{x}$  is calculated as  $\mathbf{X} \in \mathbb{R}^M$  using Eq. (1) and Eq. (2). In the wavelet domain, a convolutional block with two parallel branches is designed to extract features at different scales. The left branch consists of three consecutive 1D convolutional layers, each using a kernel size of 3. In contrast, the right branch features a one-by-one convolutional layer. The combination of different kernel sizes and processing depths allows for more comprehensive feature extraction from the wavelet domain.

In the convolutional block, each convolutional layer is followed by an adaptive hard-thresholding (AHT) nonlinearity.

Unlike the fixed threshold and slope used in conventional hard-thresholding (HT) [27] and soft-thresholding (ST) functions [28], the AHT layer introduces the trainable threshold  $C_k$  and slope  $\beta_k$  to adaptively suppress small entries and scale (denoise) large coefficients. It is defined as:

$$\hat{X}_k = (\mathcal{E}_{\mathcal{T}}(\tilde{X}_k) + C_k \cdot \text{sign}(\mathcal{E}_{\mathcal{T}}(\tilde{X}_k))) \cdot \beta_k, \quad (3)$$

where  $\mathcal{E}_{\mathcal{T}}(\tilde{X}_k) = \text{sign}(\tilde{X}_k) \cdot \text{ReLU}(|\tilde{X}_k| - C_k)$  is the soft-thresholding function.  $\tilde{X}_k$  is the convolutional layer output.  $C_k$  and  $\beta_k$  are optimized using the back-propagation algorithm [29]–[32], where  $0 \leq k \leq M-1$ . The AHT is depicted in Fig. 3.

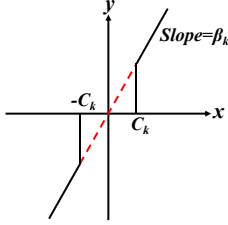


Fig. 3. Adaptive hard-thresholding nonlinearity.

#### Decoder Part of the AAELWTL:

The output of the LWT layer is quantized for transmission as described in Subsection III-C. After receiving the quantized data, the decoder starts with the ILWT to convert data from the wavelet domain back to the time domain. The transformed data  $\bar{\mathbf{x}}$  then passes through three separate linear layers and two tanh activation functions for bearing data reconstruction. Furthermore, a residual jump allows  $\bar{\mathbf{x}}$  to bypass the intermediate layers and connect directly to the next linear layer, preserving crucial information and promoting more efficient training by mitigating vanishing gradient issues.

#### B. Offline model training

To improve compression efficiency, a sparsity penalty-based cost function is designed to enforce sparsity in the latent space coefficients. Assume the LWT layer output is  $\mathbf{z} \in \mathbb{R}^M$ . First, we define the activity of  $z_k$  as follows:

$$\hat{z}_k = \delta(\mathbf{z})_k = \frac{e^{|z_k|}}{\sum_{i=0}^{M-1} e^{|z_i|}}, k = 0, 1, \dots, M-1, \quad (4)$$

where  $\delta(\cdot)$  represents the softmax function. Given that the Kullback–Leibler divergence (KLD) [33]–[36] quantifies the difference between two probability distributions, we utilize it as the sparsity regularization term:

$$\sum_{k=0}^{M-1} \text{KLD}(\lambda || \hat{z}_k) = \sum_{k=0}^{M-1} \lambda \log \frac{\lambda}{\hat{z}_k} + (1 - \lambda) \log \frac{1 - \lambda}{1 - \hat{z}_k}, \quad (5)$$

where  $\lambda$  stands for a sparsity parameter. Consequently, the total loss function is formulated as a weighted sum of the mean squared error and the KLD:

$$\text{Loss} = \frac{1}{M} \sum_{k=0}^{M-1} (x_k - y_k)^2 + \omega \sum_{k=0}^{M-1} \text{KLD}(\lambda || \delta(\mathbf{z})_k), \quad (6)$$

where  $x_k$  and  $y_k$  denote the input and output element, respectively.  $\omega$  represents the weight of the KLD term. Additionally, a threshold  $\phi$  is set. During training, when the proportion of non-zero coefficients in  $\mathbf{z}$  exceeds  $\phi$ , the training is terminated. This strategy helps eliminate small redundant coefficients.

#### C. Binary Data Storage and/or Transmission

To optimize the transmission rate during the testing or transmission phase, the outputs of the LWT layer are converted from floating-point values to integers, as integers utilize fewer bits in memory than floating-point representations. The data conversion is computed as follows:

$$\tilde{\mathbf{z}} = \text{Round}(10^\mu \cdot \mathbf{z}/\alpha), \quad (7)$$

where the parameters  $\mu$  and  $\alpha$  are utilized to control the compression ratio.  $\text{Round}(\cdot)$  stands for the integer rounding function. Next, Run-Length Encoding (RLE) [37] and Huffman Coding [38] are combined to enhance data compression and convert data into bitstreams. RLE first simplifies the data by encoding consecutive zeroes as a single zero followed by the count of repetitions. Huffman Coding is subsequently applied to the RLE output, assigning variable-length codes based on the statistical frequency of symbols. After that, the encoded data is transmitted to the decoder for reconstruction.

## IV. EXPERIMENTAL RESULTS

In this work, the MFPT [17] and XJTU [18] datasets are employed to evaluate the bearing data compression performance of the proposed method. In the MFPT dataset, the record “baseline\_1” was selected for the compression experiment, with a sampling rate of 97,656 Hz. For the XJTU dataset, we used record “bearing\_1\_1”, where the data was sampled at 25.6 kHz. To achieve a tradeoff between compression efficiency and reconstruction accuracy,  $\mu$ ,  $\alpha$ ,  $\omega$  and  $\phi$  as 3, 4, 10 and 0.6. Furthermore, the model is trained using a batch size of 30 with a learning rate of 0.001. Models are evaluated on the following metrics: the compression ratio (CR), percent root mean square difference (PRD), normalized percent root mean square difference (PRDN), root mean square error (RMSE), and quality score (QS) [39]. As the CR and QS rise, the compression efficiency and quality improve, while the disparity between the reconstructed signal and the original signal diminishes with a lower PRD, PRDN, and RMSE.

The sparse autoencoder (SAE) [33], DCT perceptron (DCTP) [40], and asymmetrical autoencoder with a sparsifying discrete cosine Stockwell transform layer (AEDCST) [16] are selected as comparison methods given that they all have low complexity encoders for bearing data compression.

Table I summarizes the bearing data compression performance of the proposed approach versus the other three state-of-the-art methods on the MFPT and XJTU datasets. In this experiment, the top 20% of the MFPT dataset is utilized for model training, while the models are evaluated on the XJTU dataset and the remaining 80% of the MFPT dataset. Compared to AEDCST, AAELWTL reduces PRD from 34.03 to 17.29 (49.19%) and RMSE from 8.17 to 4.15 (49.20%). The

TABLE I  
BEARING DATA COMPRESSION RESULTS. ALL METHODS ARE TRAINED ON THE MFPT DATASET.

Test Data	Metrics	SAE	DCTP	AEDCST	AAELWTL
MFPT	CR	7.57	9.23	9.73	<b>9.91</b>
	PRD	30.44	19.89	34.03	<b>17.29</b>
	PRDN	30.81	20.13	34.44	<b>17.50</b>
	RMSE	7.31	4.77	8.17	<b>4.15</b>
	QS	0.25	0.46	0.29	<b>0.57</b>
XJTU	CR	9.46	27.94	29.84	<b>31.37</b>
	PRD	29.89	22.72	32.93	<b>16.36</b>
	PRDN	29.89	22.72	32.93	<b>16.36</b>
	RMSE	7.64	5.81	8.41	<b>4.18</b>
	QS	0.32	1.23	0.91	<b>1.92</b>

reason is that AAELWTL incorporates more linear layers and nonlinear activation functions in the decoder than AEDCST, resulting in improved data reconstruction accuracy. Additionally, AAELWTL is superior to DCTP in terms of a higher CR and a lower PRD. It is because AAELWTL implements an adaptive hard-thresholding layer, which effectively removes redundant data while appropriately scaling large coefficients within the wavelet domain. Therefore AAELWTL has a better compression efficiency. Besides, AAELWTL outperforms SAE. SAE works as a low-pass filter. However, AAELWTL not only preserves key coefficients in the low-frequency band but also retains significant values in the high-frequency band, as shown in Fig. 4, thereby enhancing its reconstruction accuracy.

Fig. 4 illustrates the comparison between original and reconstructed signals in both the time and frequency domains. In the time domain, the reconstructed signal closely aligns with the original signal. Similarly, in the frequency domain, both signals show strong overlap. This consistent performance across both domains demonstrates that AAELWTL effectively maintains the important temporal and frequency features of the signal during the data compression process.

Table II presents ablation experimental results, where different configurations are evaluated for their impact on compression performance. When the sparsity penalty and linear

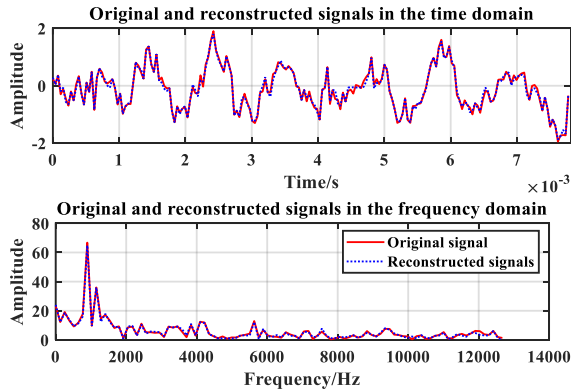


Fig. 4. Comparison between the original data (red solid line) and the reconstructed data (blue dashed line) in the time domain and the frequency domain on the XJTU dataset.

TABLE II  
ABLATION EXPERIMENTAL RESULT ON THE MFPT DATASET.

Metrics	No penalty	No linear	ST	HT	AAELWTL
CR	9.80	9.90	9.67	9.84	<b>9.91</b>
PRD	17.38	19.33	42.32	17.30	<b>17.29</b>
PRDN	17.60	19.57	42.84	17.51	<b>17.50</b>
RMSE	4.17	4.64	10.16	4.15	<b>4.15</b>
QS	0.56	0.51	0.23	0.57	<b>0.57</b>

TABLE III  
THE MACs AND NUMBER OF TRAINABLE PARAMETERS.

Algorithm	MACs	Parameters
SAE	107,520	3,120
DCTP	147,840	130
AEDCST	160,496	5,312
Proposed method	<b>60,480</b>	<b>74</b>

layers are removed from the proposed model, the performance deteriorates, indicating these components play a crucial role in enhancing the compression efficiency and reconstruction capability of AAELWTL. Moreover, AAELWTL with the AHT layer demonstrates superior compression performance compared to AAELWTL with either HT or ST layer. Although the ST layer can scale large coefficients, its fixed scaling factor restricts its adaptability to varying data characteristics. In contrast, the AHT layer introduces a trainable slope, allowing for dynamic adjustment of the data. Additionally, the original HT layer lacks the capability to scale large entries, further limiting its compression efficiency.

Table III compares the computational complexity (measured in Multiply-Accumulates (MACs)) and the number of trainable parameters on the encoder side. Among all the models, AAELWTL exhibits the lowest MACs and the fewest trainable parameters. The reduced computational complexity and parameter count contribute to lower memory consumption and hardware costs, making the model more feasible for deployment in resource-limited sensors.

## V. CONCLUSION

This study proposes an asymmetrical autoencoder with an LWT layer for bearing sensor data compression. A single convolutional layer cannot be trained in conjunction with an adaptive hard-thresholding nonlinearity. By imposing the convolutional layer after the fixed LWT, we can simultaneously train both the thresholds and the convolutional layer, allowing the model to adapt to the data while enhancing the compression ability of the encoder module. Furthermore, the decoder features a more sophisticated architecture, consisting of the ILWT, three linear layers, and two tanh activation functions, which significantly improve its reconstruction performance. The experimental results demonstrate that the proposed method surpasses other state-of-the-art models in terms of CR, PRD, PRDN, RMSE, and QS. Moreover, the AAELWTL encoder has a low computational complexity and a lower number of trainable parameters, making it well-suited for deployment on sensors to efficiently compress bearing data.

## REFERENCES

- [1] Maruti Khaire, "Role of bearings in new generation automotive vehicles: powertrain," in *Advanced Applications of Hydrogen and Engineering Systems in the Automotive Industry*. IntechOpen, 2020.
- [2] Cédric Peeters, Patrick Guillaume, and Jan Helsen, "Vibration-based bearing fault detection for operations and maintenance cost reduction in wind energy," *Renewable Energy*, vol. 116, pp. 74–87, 2018.
- [3] Yasir Hassan Ali, Roslan Abd Rahman, and Raja Ishak Raja Hamzah, "Acoustic emission signal analysis and artificial intelligence techniques in machine condition monitoring and fault diagnosis: a review," *Jurnal Teknologi*, vol. 69, no. 2, 2014.
- [4] Yasir Hassan Ali, Salah M Ali, RA Rahman, and Raja Ishak Raja Hamzah, "Acoustic emission and artificial intelligent methods in condition monitoring of rotating machine—a review," in *National Conference for Postgraduate Research*, 2016.
- [5] Mohammad Badrul Hossain and Md Nowroz Junaed Rahman, "An empirical analysis on lossless compression techniques," in *International Conference on Computer and Communication Engineering*. Springer, 2023, pp. 158–170.
- [6] Yumeng Shi, Shihao Bai, Xiuying Wei, Ruihao Gong, and Jianlei Yang, "Lossy and lossless (12) post-training model size compression," in *Proceedings of the IEEE/CVF International Conference on Computer Vision*, 2023, pp. 17546–17556.
- [7] Amal Altamimi and Belgacem Ben Youssef, "Lossless and near-lossless compression algorithms for remotely sensed hyperspectral images," *Entropy*, vol. 26, no. 4, pp. 316, 2024.
- [8] Qingqing Huang, Baoping Tang, Lei Deng, and Jiaxu Wang, "A divide-and-compress lossless compression scheme for bearing vibration signals in wireless sensor networks," *Measurement*, vol. 67, pp. 51–60, 2015.
- [9] Haotian Yu, Yaguang Yang, Daibo Zhang, Qiliang Zhang, and Zhiqiang Li, "Vlsi design for adjustable compression rate in lossless/lossy compression of eeg signal," *Microelectronics Journal*, vol. 148, pp. 106193, 2024.
- [10] Phuong Thi Dao, Xue Jun Li, and Hung Ngoc Do, "Lossy compression techniques for eeg signals," in *2015 International Conference on Advanced Technologies for Communications (ATC)*. IEEE, 2015, pp. 154–159.
- [11] Garry Higgins, Stephen Faul, Robert P McEvoy, Brian McGinley, Martin Glavin, William P Marnane, and Edward Jones, "Eeg compression using jpeg2000: How much loss is too much?," in *2010 Annual International Conference of the IEEE Engineering in Medicine and Biology*. IEEE, 2010, pp. 614–617.
- [12] Yingyi Luo, Talha M Khan, Emadeldeen Hamdan, Xin Zhu, Hongyi Pan, Didem Ozevin, and A Enis Cetin, "An sputtering parameter estimation using a multichannel parallel dct neural network," in *2024 IEEE 42nd VLSI Test Symposium (VTS)*. IEEE, 2024, pp. 1–5.
- [13] Emadeldeen Hamdan, Xin Zhu, Didem Ozevin, Pai-Yen Chen, and A Enis Cetin, "Effect of data compression on crack location prediction using acoustic emission sensor arrays," in *2024 International Conference on Electromagnetics in Advanced Applications (ICEAA)*. IEEE, 2024, pp. 1–1.
- [14] Yuhua Yin, Zhiliang Liu, Mingjian Zuo, Zetong Zhou, and Junhao Zhang, "A three-dimensional vibration data compression method for rolling bearing condition monitoring," *IEEE Transactions on Instrumentation and Measurement*, vol. 72, pp. 1–10, 2023.
- [15] Wei Guo and W Tse Peter, "A novel signal compression method based on optimal ensemble empirical mode decomposition for bearing vibration signals," *Journal of sound and vibration*, vol. 332, no. 2, pp. 423–441, 2013.
- [16] Xin Zhu, Daoguang Yang, Hongyi Pan, Hamid Reza Karimi, Didem Ozevin, and Ahmet Enis Cetin, "A novel asymmetrical autoencoder with a sparsifying discrete cosine stockwell transform layer for gearbox sensor data compression," *Engineering Applications of Artificial Intelligence*, vol. 127, pp. 107322, 2024.
- [17] "Society for machinery failure prevention technology," <https://mfpt.org/fault-data-sets/>, 2019, Accessed: September 2019.
- [18] "Xjtu-sy bearing datasets," <http://biaowang.tech/xjtu-sy-bearing-datasets/>, 2019, Accessed: September 2019.
- [19] Chai W Kim, Rashid Ansari, and A Enis Cetin, "A class of linear-phase regular biorthogonal wavelets," in *IEEE ICASSP Conference*, 1992, vol. 92, pp. 673–676.
- [20] Majid Rabbani and Rajan Joshi, "An overview of the jpeg 2000 still image compression standard," *Signal processing: Image communication*, vol. 17, no. 1, pp. 3–48, 2002.
- [21] Wim Sweldens, "Wavelets and the lifting scheme: A 5 minute tour," *ZAMM-Zeitschrift für Angewandte Mathematik und Mechanik*, vol. 76, no. 2, pp. 41–44, 1996.
- [22] Ingrid Daubechies and Wim Sweldens, "Factoring wavelet transforms into lifting steps," *Wavelets in the Geosciences*, pp. 131–157, 2005.
- [23] Omer N Gerek and A Enis Cetin, "Adaptive polyphase subband decomposition structures for image compression," *IEEE Transactions on Image Processing*, vol. 9, no. 10, pp. 1649–1660, 2000.
- [24] Omer N Gerek and A Enis Cetin, "Lossless image compression using an edge adapted lifting predictor," in *IEEE International Conference on Image Processing 2005*. IEEE, 2005, vol. 2, pp. II–730.
- [25] Omer N Gerek and A Enis Cetin, "A 2-d orientation-adaptive prediction filter in lifting structures for image coding," *IEEE Transactions on Image Processing*, vol. 15, no. 1, pp. 106–111, 2005.
- [26] Jun-Hyuk Kim, Jun-Ho Choi, Jaehyuk Chang, and Jong-Seok Lee, "Efficient deep learning-based lossy image compression via asymmetric autoencoder and pruning," in *ICASSP 2020-2020 IEEE International Conference on Acoustics, Speech and Signal Processing (ICASSP)*. IEEE, 2020, pp. 2063–2067.
- [27] Hu Li, Songsong Li, Jiao Sun, Benchi Huang, Jiaqi Zhang, and Mingyang Gao, "Ultrasound signal processing based on joint gwo-vmd wavelet threshold functions," *Measurement*, vol. 226, pp. 114143, 2024.
- [28] Huan Wang, Wenjun Luo, Zhiliang Liu, Junhao Zhang, and Mingjian Zuo, "Fourier feature refiner network with soft thresholding for machinery fault diagnosis under highly noisy conditions," *IEEE Internet of Things Journal*, 2024.
- [29] Lihua Wang, Wenjing Ye, Yanjuan Zhu, Fan Yang, and Yueting Zhou, "Optimal parameters selection of back propagation algorithm in the feedforward neural network," *Engineering Analysis with Boundary Elements*, vol. 151, pp. 575–596, 2023.
- [30] Mirza Cilimkovic, "Neural networks and back propagation algorithm," *Institute of Technology Blanchardstown, Blanchardstown Road North Dublin*, vol. 15, no. 1, 2015.
- [31] Yann LeCun, D Touresky, G Hinton, and T Sejnowski, "A theoretical framework for back-propagation," in *Proceedings of the 1988 connectionist models summer school*, 1988, vol. 1, pp. 21–28.
- [32] Arjen Van Ooyen and Bernard Nienhuis, "Improving the convergence of the back-propagation algorithm," *Neural networks*, vol. 5, no. 3, pp. 465–471, 1992.
- [33] Andrew Ng et al., "Sparse autoencoder," *CS294A Lecture notes*, vol. 72, no. 2011, pp. 1–19, 2011.
- [34] John R Hershey and Peder A Olsen, "Approximating the kullback leibler divergence between gaussian mixture models," in *2007 IEEE International Conference on Acoustics, Speech and Signal Processing-ICASSP'07*. IEEE, 2007, vol. 4, pp. IV–317.
- [35] Fernando Pérez-Cruz, "Kullback-leibler divergence estimation of continuous distributions," in *2008 IEEE international symposium on information theory*. IEEE, 2008, pp. 1666–1670.
- [36] Dmitry I Belov and Ronald D Armstrong, "Distributions of the kullback–leibler divergence with applications," *British Journal of Mathematical and Statistical Psychology*, vol. 64, no. 2, pp. 291–309, 2011.
- [37] Shahin Akhter and MA Haque, "Ecg compression using run length encoding," in *2010 18th European Signal Processing Conference*. IEEE, 2010, pp. 1645–1649.
- [38] Mamta Sharma et al., "Compression using huffman coding," *IJCSNS International Journal of Computer Science and Network Security*, vol. 10, no. 5, pp. 133–141, 2010.
- [39] Chandan Kumar Jha and Maheshkumar H Kolekar, "Electrocardiogram data compression using dct based discrete orthogonal stockwell transform," *Biomedical Signal Processing and Control*, vol. 46, pp. 174–181, 2018.
- [40] Hongyi Pan, Emadeldeen Hamdan, Xin Zhu, Salih Atici, and Ahmet Enis Cetin, "Multichannel orthogonal transform-based perceptron layers for efficient resnets," *IEEE Transactions on Neural Networks and Learning Systems*, 2024.